Aerospace Science and Technology 73 (2018) 32–47

Contents lists available at ScienceDirect

Aerospace Science and Technology

www.elsevier.com/locate/aescte

Conceptual design of a Blended Wing Body MALE UAV

P. Panagiotou, S. Fotiadis-Karras, K. Yakinthos *

Laboratory of Fluid Mechanics & Turbomachinery, Dept. of Mechanical Engineering, Aristotle University of Thessaloniki, 54124, Thessaloniki, Greece

ARTICLE INFO

Article history:
Received 1 September 2017
Received in revised form 19 November 2017
Accepted 20 November 2017
Available online 24 November 2017

Keywords:
BWB
UAV
Design
Layout
Conceptual
Trade studies

ABSTRACT

The current work is an aerodynamic design study of a Blended Wing Body (BWB) Medium-Altitude-Long-Endurance (MALE) Unmanned-Aerial-Vehicle (UAV). Using a combined approach of presizing tools and computational simulations, a step-by-step layout design study was conducted to define the key layout characteristics and select the optimal airframe-engine combination. Trade studies were also carried out to optimize the aerodynamic performance and stability. The traditional sizing and aerodynamic estimation methods were adopted to incorporate the characteristics of the BWB platform, whereas CFD computations were employed in order to calculate the aerodynamic and stability coefficients, during the layout comparison and trade studies. Drawings and tables are provided to show the progression of the design study at each stage. The performance specifications are also compared with a conventional UAV platform to point out the main advantages and disadvantages of the BWB for MALE UAV applications.

1. Introduction

The Blended Wing Body (BWB) is a tailless design that integrates the wing and the fuselage and was initially conceived towards the end of the 20th century to serve as a novel platform for high-speed subsonic commercial airliners [1,2]. In the general case, it consists of a middle section (center body or fuselage) and an outer section (wing), whereas the part in between is the blending area, where the center body smoothly connects (blends) into the wing geometry (Fig. 1). It features several advantages, such as low wetted area to internal volume ratio, potential for elliptic lift distribution, smooth varying cross-section distribution, and adequate space for engine installation on the top of the airframe, to name a few. Hence, there is a wide number of existing studies mainly concerning the BWB as a commercial airliner, dealing with issues related to aerodynamics, structures, and control [1,3–9]. Despite its unique aspects and potential though, the BWB is not expected to enter service before the late 2030s [10], because its revolutionary shape is also responsible for a number of issues that have to do with passenger safety and comfort. Indicatively, cabin pressurization, passenger safety and evacuation are some of the most important issues and, despite the ongoing research [10–13], the BWB concept cannot be considered as a viable option in the commercial airliner layout designers' arsenal, at least for the time being.

However, such a platform can be a promising candidate for other aeronautical applications as well. For example, as also mentioned in a recent announcement by Boeing, the blended wing body can also serve as a cargo airplane [14,15]. There are some issues that have to be solved before this BWB application reaches the skies in this case also, such as the mid-flight opening of the cargo door and the effect it has on the stability of the aircraft. Another possible application is a smaller-scale unmanned platform, as also mentioned in [16]. Unmanned Aerial Vehicles (UAVs) have many advantages, which mainly arise from the lack of crew on board, and can provide solutions to a wide range of applications. Hence, at the present, they are already being operated by several military forces, and civilian organizations [17], whereas there is a wide number of studies that deal with UAV design and optimization [18–24]. Therefore, an innovation in terms of geometry could aid in improving their performance characteristics and, consequently, their operating capabilities. Such an innovative configuration is the BWB. With its aforementioned advantages (increased aerodynamic efficiency and internal volume) it can potentially im-

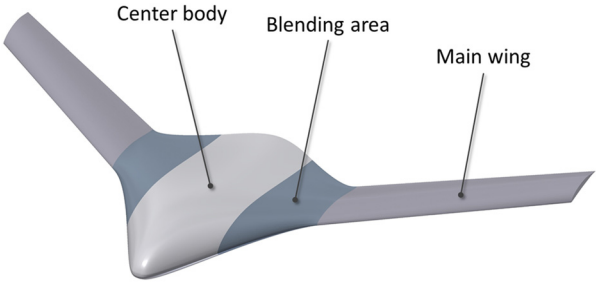

Fig. 1. The BWB concept.

* Corresponding author.
E-mail address: kyak@auth.gr (K. Yakinthos).

https://doi.org/10.1016/j.ast.2017.11.032
1270-9638/

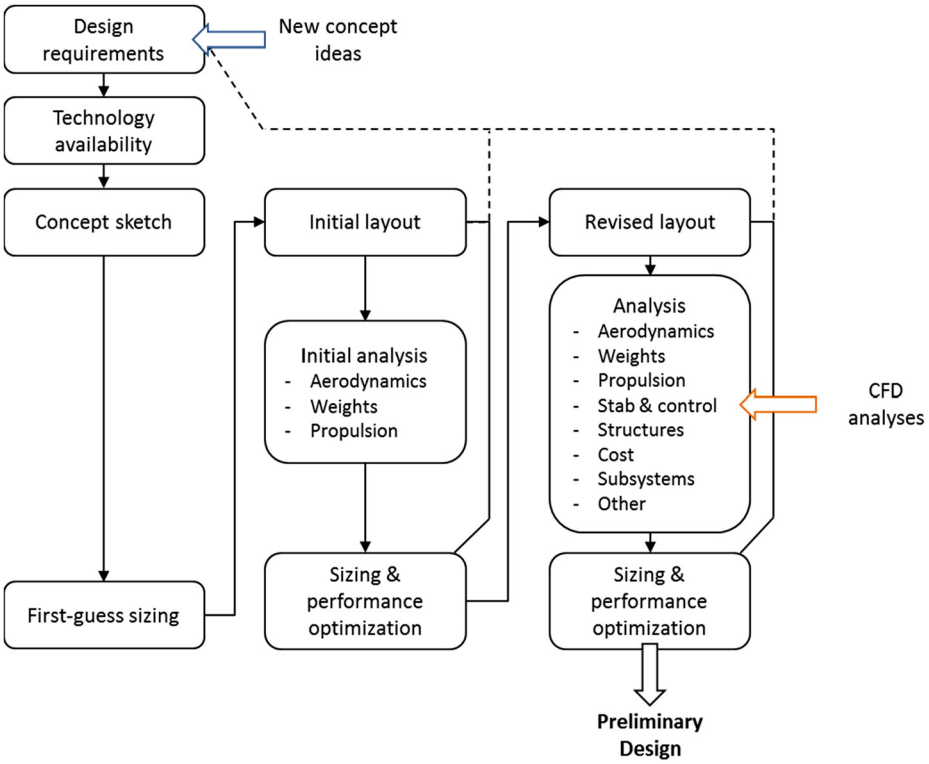

Fig. 2. Conceptual design roadmap.

prove the performance and the operational specifications of aircraft that operate in low subsonic speeds as well, and more specifically in the incompressible flow regime, as is the case of most UAVs [18,25–27].

There is a number of studies, which examine the BWB geometry as a UAV concept either from a designer's perspective or experimentally. For example, Lehmkuehler et al. [16] present the design and testing of a BWB UAV concept, whereas in [28] an experimental study of a BWB UCAV model is shown, including force balance measurements and surface pressure measurements. Moreover, Wisnoe et al. [29,30] in their studies conducted CFD analyses and experimental studies on two BWB configurations. To the best of our knowledge though, all of the BWB UAV-related design studies concern a single concept, and no study goes through a step-by-step design procedure, as the ones presented in [19,20] for conventional configurations. A BWB-related parametric study was recently made in [31], but emphasized on aerodynamics and did not include design considerations.

In the current work, the layout design study of a BWB MALE UAV is presented. The mission requirements correspond to the specifications of a typical surveillance MALE UAV, as also described in [18]. A step-by-step presentation of the design procedure is made, including the presizing methods and CFD methodology. Emphasis is given on the unique aspects of the BWB configuration and the way those are incorporated in the design methodology. The presentation starts with the initial calculations, the layout comparison and engine selection study, to come up with a first configuration i.e., the Dash-One. A number of trade studies and a comparison with a conventional configuration is then conducted to investigate the potential and the limits of the BWB configuration as a MALE UAV platform.

2. Conceptual design methodology

For the conceptual design procedure described in this study, a custom sizing methodology is employed, which combines the traditional aircraft and UAV presizing methods with computational simulations. Moreover, some special considerations are made to incorporate the aspects of BWB into the design procedure, such as the weight estimation and aerodynamic coefficient prediction methods. In the following chapters both the layout design methods and the CFD methodology are briefly described, whereas Section 2.3 is dedicated to the BWB-related elements of the design procedure.

2.1. Traditional sizing methods

Considering the presizing calculations an in-house tool was employed, which has been developed in the Laboratory of Fluid Mechanics and Turbomachinery (LFMT), at the Department of Mechanical Engineering, at the Aristotle University of Thessaloniki (AUTH), Greece. Based on aircraft design methods, such as the ones described in [2,32,33], it also includes the aspects of unmanned aircraft design and is a combination of analytical and semi-empirical presizing methods. It can be used to carry out a complete layout design study and aerodynamic analysis, and has been validated on commercial airliners and unmanned aerial vehicle configurations [18,34]. A roadmap of the conceptual design tool is presented in Fig. 2.

At first, the mission requirements are defined and, along with any new concept ideas and taking into account available technology, they serve as the design guidelines. Then, the first presizing calculations are conducted, based mostly on semi-empirical relations and statistical data, as well as some early concept sketches. The next step is to estimate some key performance parameters and layout elements, such as airfoil specifications, wing area, and propulsion specifications, that serve as the base upon which the detailed configuration layouts/candidates are drawn. Those detailed layouts allow for the refined weight estimations and aerodynamic coefficient predictions to be conducted, which in turn are used to carry out detailed performance analysis studies. Based on the refined numbers, the various configurations are compared and the

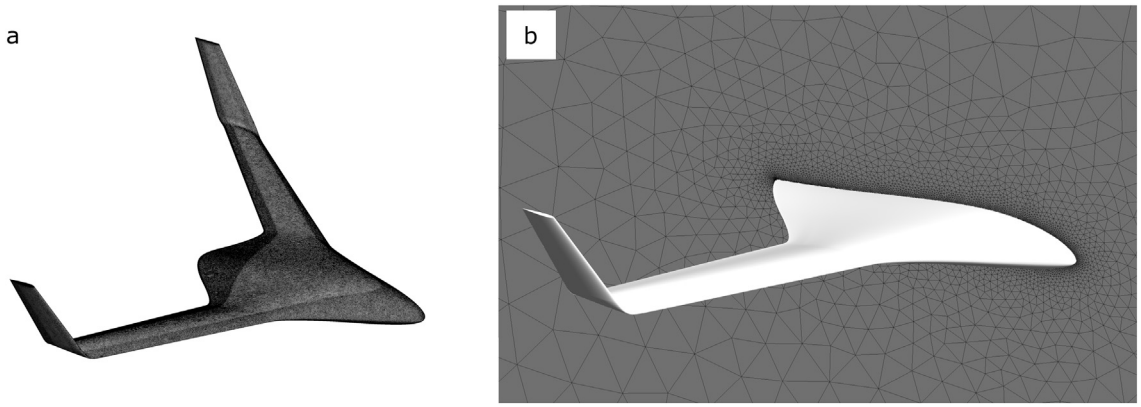

Fig. 3. Computational mesh on the surface (a) and around (b) a BWB configuration.

designer comes up with the most suitable configuration, i.e. the Dash-One. The final step before going into the next design phase, i.e. the preliminary design phase, is to conduct trade studies and fine-tune the characteristics of the Dash-One, to make sure that the basic layout considerations have been successfully addressed during the conceptual design.

2.2. CFD methodology

The CFD analysis was conducted using the ANSYS CFX commercial software (ANSYS@ Scientific Research, Release 18.1). An unstructured grid was generated around each of the examined configurations, consisting of approximately 6,000,000 computational nodes (Fig. 3). The Reynolds-Averaged Navier–Stokes (RANS) equations were solved, coupled with the Spalart–Allmaras [35] turbulence model, to ensure a high accuracy in the calculation of the normal and shear stresses acting on the wing's surface. More specifically, the RANS in Einstein notation can be written as

$$\rho \overline{u}_j \frac{\partial \overline{u}_i}{\partial x_j} = \frac{\partial}{\partial x_j}\left[-\overline{p}\delta_{ij} + \mu\left(\frac{\partial \overline{u}_i}{\partial x_j} + \frac{\partial \overline{u}_j}{\partial x_i}\right) - \rho\overline{u_i' u_j'}\right] \tag{1}$$

In the Spalart–Allmaras turbulence model, the Reynolds stresses tensor is given by $-\overline{u_i' u_j'} = 2\nu_t S_{ij}$, ignoring the term containing the turbulence kinetic energy. S_{ij} is the strain-rate tensor and ν_t is the eddy viscosity, which is given by

$$\nu_t = \tilde{\nu} f_{v1} \tag{2}$$

Note that $\tilde{\nu}$ is the "working variable" of the model, and obeys the transport equation

$$\frac{D\tilde{\nu}}{Dt} = c_{b1}[1 - f_{t2}]S\tilde{\nu} + \frac{1}{\sigma}\left[\nabla \cdot \left((\nu + \tilde{\nu})\nabla\tilde{\nu}\right) + c_{b2}(\nabla\tilde{\nu})^2\right] - \left[c_{w1} f_w - \frac{c_{b1}}{\kappa^2} f_{t2}\right]\left[\frac{\tilde{\nu}}{d}\right]^2 + f_{t1}\Delta U^2 \tag{3}$$

Details about the variables and the various coefficients can be found in [35].

A second order upwind scheme was used for both the discretized momentum and turbulence model equations, whereas the inlet turbulence intensity was set at 1% and the eddy viscosity ratio at 0.2, representing typical flight conditions [36]. A steady-state approach was employed due to computational resources limitations. 20 inflation layers were generated on the walls of the aerial vehicle, the first of which was placed at $2.5{\cdot}10^{-5}$ m from the wall to ensure that the $y+$ at the wall will not exceed a value of 5, so that the local, low-Reynolds boundary layer phenomena in the wall region can be accurately modeled. It should be noted that the CFD approach was vital in this BWB conceptual design study, due to the fact that other methods, such as existing textbook and low-fidelity methods, such as Vortex-Lattice-Method (VLM), cannot accurately predict the aerodynamic behavior of this type of configuration [31]. More specifically, starting from the point where the different layouts were drawn, CFD was the main tool for predicting the much-needed aerodynamic and stability coefficients.

To carry out the CFD computations, 3D representations of the configurations are drawn. In this work, a parametric 3D CAD approach was employed to ensure that the configurations will be accurately modeled. Hence, a custom parametric design tool developed in the LFMT was used, in a synergetic approach with a commercial software (Autodesk Inventor®). The methodology is presented in detail in [31].

2.3. BWB considerations

Since, by definition, the BWB is a novel configuration, there are some special considerations that had to be made for the purposes of this study. Those considerations mainly refer to weight estimation and aerodynamic coefficient methods, as well as some unique layout design elements. More specifically:

Layout design

The absence of a conventional fuselage means that the center body sizing is primarily driven by internal volume constraints. That is, the selection of the center body airfoil profiles must ensure adequate internal volume for the payload equipment and fuel, before considering other important parameters, such as aerodynamic and stability.

Moreover, reflexed camber airfoils are employed for longitudinal stability purposes [1,6], to reduce the pitch-down moment that would otherwise increase the trimming requirements.

In addition, the BWB is essentially a tailless configuration. That is, the platform does not have a part dedicated to pitch or yaw control. To counter this problem a designer may add extra surfaces, such as vertical fins or canards, but even in that case the available tail arms are limited.

Weight prediction methods

The majority of the weight prediction methods are based on statistical data and empirical relations based on conventional configurations, such as tube-and-wing aircraft. Applying these methods on a novel configuration would lead to wrong and misleading weight estimations when it comes to predicting empty weight, and consequently, the Gross Takeoff Weight (GTOW or W_0). During the conceptual design though, those weight estimations are the only

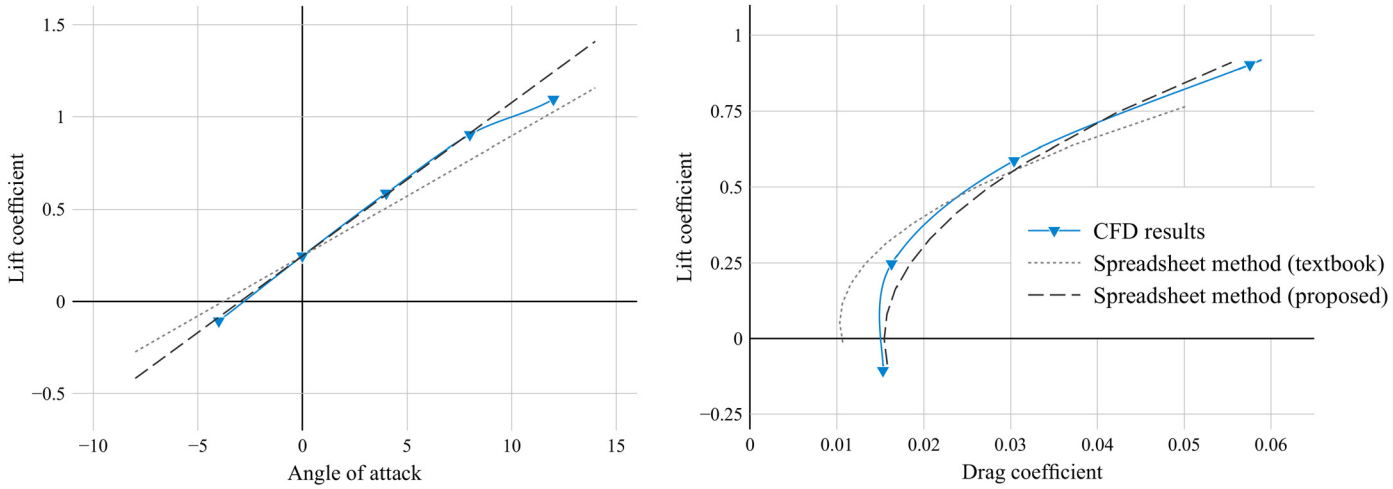

Fig. 4. Aerodynamic coefficient prediction using the spreadsheet tools (textbook vs. proposed methodologies) and comparison with CFD data from the reference configuration of [31].

source of weight-related information and weight is probably the most important parameter, affecting every aspect of the design. Moreover, the very limited number of available BWB UAVs does not allow for the extraction of dedicated statistical data, at least not yet. Hence, the corresponding correction factors provided in [32] were eventually employed, i.e. fudge factors equal to 0.768 and 0.774 for the wing and fuselage weight estimates respectively. Note that it is the center body geometry that is treated as the fuselage, in the case of the BWB. More specifically, equations (4) and (5) were used to estimate the empty weight for the wing and center body (fuselage) parts, during the refined weight estimation procedure:

$$W_{(wing)} = F_c F_{(BWB,\ wing)} 0.036 S_w^{0.758} W_{fw}^{0.0035} \left(\frac{A}{\cos^2 \Lambda}\right)^{0.6} \cdot q^{0.006} \lambda^{0.04} \left(\frac{100t/c}{\cos \Lambda}\right)^{-0.3} (N_z W_{dg})^{0.49} \quad (4)$$

$$W_{(center\ body)} = F_c F_{(BWB,\ center\ body)} 0.052 S_f^{1.086} (N_z W_{dg})^{0.177} \cdot L_t^{-0.051} (L/D)^{-0.072} q^{0.241} \quad (5)$$

where $F_{(BWB,\ wing)}$ and $F_{(BWB,\ center\ body)}$ are the fudge factors described above, F_c is a fudge factor related to the use of composite materials and is equal to 0.85, whereas the rest of the variables are explained in [32].

Aerodynamic coefficient estimation method

The traditional textbook aerodynamic coefficient estimation methods cannot accurately predict the aerodynamic performance of a BWB platform, as explained in [31]. The percentage error may reach as much as 50%, and the main reason appears to be that they do not take into account the contribution of the center body to the total Lift force, which also has a considerable impact on the Drag force. To deal with this issue, a modification was made to the aerodynamic coefficient estimation method by "splitting" the BWB configuration to the wing platform and the center body geometry. That way, and by treating them both as separate lifting bodies, the methods from [33] are applied to calculate the Lift and Drag components. The sub-components are in turn added, as presented in equations (6) and (7).

$$C_L = \frac{C_{L_{(wing)}} S_{(wing)} + C_{L_{(center\ body)}} S_{(center\ body)}}{S} \quad (6)$$

$$C_D = \frac{C_{D_{(wing)}} S_{(wing)} + C_{D_{(center\ body)}} S_{(center\ body)}}{S} \quad (7)$$

where S is the reference area.

To validate the proposed methodology, the CFD results from [31] were employed. More specifically a comparison between CFD results, the textbook methodology, and proposed methodology is shown in Fig. 4.

The curve corresponding to the proposed methodology is closer to the CFD results, than the one corresponding to the textbook method, at both charts presented in Fig. 4. This is an indication that the modification made to the aerodynamic coefficient estimation methodology works. It should be noted though that this methodology was only used to get quick estimates of the aerodynamic coefficients at the first steps of the design procedure. As the design progressed, and different configurations were examined, the prediction accuracy of the proposed method deviated as much as 10% from the CFD results.

3. Layout design study – results

In this section, a detailed presentation of the design procedure is made, including the mission requirements definition, the development of three different layout configurations and the corresponding comparative study, the engine selection study, and the optimization and trade studies that lead to the final configuration of the conceptual design phase.

3.1. First sizing calculations and Dash-One

Requirements

The first step of an aerodynamic design study is the definition of the mission requirements of the aerial vehicle. That is, the operational requirements related, for example, to payload weight, flight endurance and flight velocities. The selected values are presented in Table 1 and correspond to a typical surveillance MALE UAV [18,25].

The payload weight refers to the total weight of the on-board electronic and surveillance equipment and must be adequately high to ensure that equipment such as radios, optical and IR sensors and on-board computers, are taken into account. The loiter speed is set at 140 km/h, whereas the loiter endurance, maximum speed and service ceiling must exceed 8 h, 200 km/h and 3 km respectively in order for the MALE UAV to be versatile and competitive as a surveillance platform. The use of composite materials

Table 1
Mission requirements.

Flight requirements	Other requirements
Payload weight = 35 kg	Inherent stability
Endurance > 8 h	Composite materials
Loiter speed = 140 km/h	Optical & IR sensors
Maximum speed ≥ 220 km/h	Retractable wings
Service ceiling ≥ 3 km	
Takeoff runway ≤ 200 m	

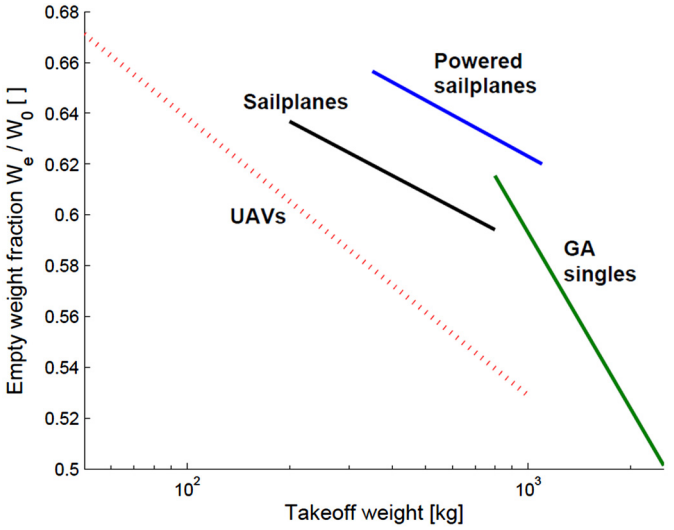

Fig. 5. Empty weight fraction curves for various types of aircraft [37].

is vital to achieve high durability at the lowest possible structural weight, whereas the retractable wings help increase the mobility of the aerial vehicle, since it can be disassembled on the ground and fit inside a cargo vehicle.

Initial sizing

Following the methodology presented in Fig. 2, the first step of the layout design study is to calculate the first weight estimate. In the case of a UAV, the GTOW is the sum of the payload weight W_p, the fuel weight W_f and the empty weight W_e (eq. (8)):

$$W_0 = W_p + W_e + W_f \tag{8}$$

The payload weight is defined by the mission requirements (Table 1). The empty weight is the UAV tare weight and in this first design stage it is estimated using historical trends and statistical data for operating aircraft with similar requirements [32,37]. More specifically, the data provided in [37] and Fig. 5 were employed, corresponding to an empty weight fraction ($\frac{W_e}{W_0}$) of 0.57. Hence, this first empty weight estimation did not take into account the BWB shape of the platform.

The fuel weight is calculated by estimating the fuel consumption for each flight segment (Fig. 6), whereas a 6% factor is taken into account for safety purposes [32]. The fuel consumption estimations are based either on statistical data or on analytical calculations, depending on the segment. For example, the Breguet equation (eq. (9)) is used to estimate the required fuel for the loiter and cruise segments:

$$R = E \cdot V = \int_{W_{i+1}}^{W_i} \frac{V}{C}\frac{L}{D}\frac{dW}{W} \tag{9}$$

where R, E are the cruise range and loiter endurance respectively, V is the respective flight velocity and C is the special fuel consumption, whereas W_i refers to the weight of the aerial vehicle at the end of the mission segment i. For this first estimate, the L/D was selected based on the "Wetted Aspect Ratio" methodology proposed by Raymer [32]. Hence, a L/D ratio of 16 was used. For C the typical values for loiter and cruise were selected [2,32], assuming as a start that a propeller-driven engine is used, as is the case with most surveillance UAVs [18,25,27].

The next step is to specify the basic aerodynamic parameters i.e. the airfoil characteristics and wing geometry parameters. Regarding the airfoil, a conventional airfoil was considered for the tip and a reflexed camber airfoil for the center body, i.e. the FX 76-MP-120 and the MH-108 respectively. Hence, based on their respective characteristics, an average value of 1.44 served as a first indication for the maximum lift coefficient, whereas an aspect ratio of 8 and taper ratio of 0.5 were selected for the main wing [2,18]. It should be noted that, to define those aerodynamic parameters, only the main wing area was used as the reference area, as shown in Fig. 7 to keep consistency with other BWB-related studies [6,31].

Two of the most important performance parameters can now be estimated, i.e. the thrust-to-weight ratio (T/W) and the wing loading (W/S). The thrust-to-weight ratio can easily be converted to the power loading ratio, which is the equivalent parameter when a propeller-powered engine is used. Based on the requirements, the corresponding presizing methods were used [2,32] to calculate the required values for every scenario (Table 2). The largest estimated value was selected for T/W and the lowest for W/S, i.e. 0.213 and 7.66 respectively.

This is the point where the initial sizing calculations end, and the development of the configuration layout of the aerial vehicle essentially initiates.

Layout comparison

In this section, the layout design of the BWB MALE UAV is drawn, based on the aerodynamic parameters and wing area estimates. In most BWB-related design studies, a single configuration

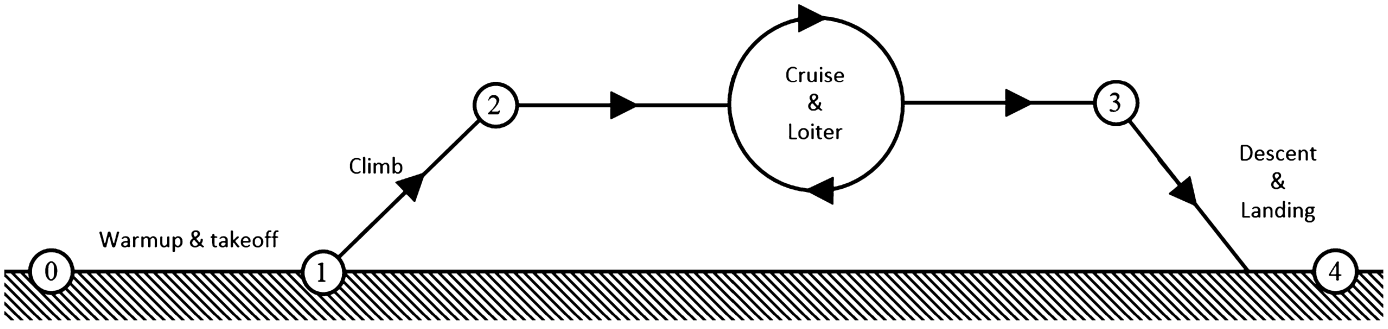

Fig. 6. Typical surveillance MALE UAV mission profile [18].

Table 2
Power loading and wing loading selection.

Mission	Wing loading	Power loading
Maximum speed	N/A	0.213
Takeoff distance	8.14	0.15
Stall	7.66	N/A
Max. ceiling	15.6	N/A

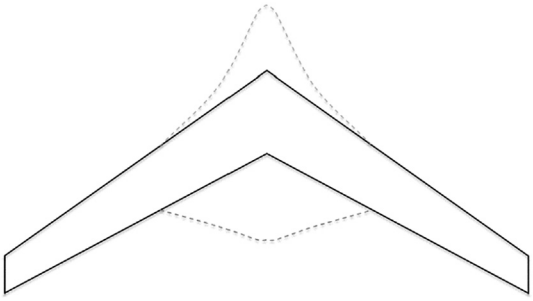

Fig. 7. Top view of the BWB planform. The aspect ratio and taper ratio definitions were based on the "main wing planform", which is drawn with a solid line.

is examined [3,16,28,38–40], with the exception of Siouris and Qin [5] where even though some parametric considerations are included in the design procedure, they are kept in sweep angle changes and deal with high-speed performance. However, in this work three different configurations were developed, each of who dealt with the stability and controllability in a different way. Separate calculations were conducted for each of the configurations, which yielded different results in terms of aerodynamic coefficients, weight estimates and, ultimately, performance parameters. Moreover, from this point onward, and for the rest of the design study, the computational simulations play a major role, since all the results related to aerodynamics and stability are calculated using CFD. The guidelines for the layout design were:

I. To meet the requirements set at the beginning of the design process.
II. To ensure adequate controllability, at the minimum cost in control surfaces size and wetted area penalty.
III. To ensure that the required equipment and fuel can fit into the hull of the designed aerial vehicle.

Regarding the airfoils, a combination of conventional profiles and reflexed camber ones were employed, for the reasons discussed in Section 2.3. Given the local Reynolds numbers, the selection criteria were the aerodynamic efficiency, maximum lift coefficient, zero lift angle of attack and maximum thickness, especially for the center body profiles. Eventually, a thick, reflexed camber airfoil was used for the center body and a thick, high camber airfoil for the wingtip. For the frame in between, i.e. the blending area, a hybrid-looking airfoil was selected, to combine performance with stability

Table 3
Layout specifications and weights comparison between the three configurations.

Plane	Airfoil type	Local Re number	Max. thickness	Max. camber
1	MH-104	$6.5{\cdot}10^6$	15.28	1.9%
2	MH-104	$3.9{\cdot}10^6$	15.28	1.9%
3	MH-18	$1.9{\cdot}10^6$	11.16	2.7%
4	FX 76-MP-120	$1.2{\cdot}10^6$	12.1	7.6%

characteristics and ensure a smooth transition from center body profiles to the wingtip ones. The above information is presented in Fig. 8 and Table 3.

Regarding the sizing of the control surfaces, the early presizing methods from [32] were employed, which yield the necessary combination of areas and lever arms for roll, pitch, and yaw stability and control. Following some initial calculations, it became evident that, since the available lever arms are relatively limited, the resulting surfaces will be considerably larger than those of a conventional configuration. The most efficient way to alleviate this issue was to design multi-functional control surfaces, like for example a combined elevator-aileron (elevon) surface, place them as far away from the symmetry plane as possible, and at the same time keep the main wing sweep angle around 35 degrees in order to move the wingtips rearwards. The way those surfaces were merged together can be described using the following simple relation (eq. (10)):

$$\sum \frac{S_i L_i}{c_i} = \bar{c}_w S_w \tag{10}$$

where c_w and S_w are the mean aerodynamic chord and reference are of the wing, whereas S_i, L_i and c_i are the reference area, lever arm and local chord of every control surface respectively.

The rest of the layout parameters and dimensions were drawn to satisfy the presizing calculations and performance parameters. It should be noted that, all three of the aforementioned guidelines were eventually taken into account. The first one (I) was essentially achieved by comparing the performance parameters with the mission requirements. For the second one (II), the dedicated presizing methods were employed for the control surface sizing, as described above. Finally, regarding the volume requirements (III), in combination with the proper selection of airfoil thickness, a validation using the 3D CAD was also conducted. The largest internal "blocks" are the payload and the fuel tank. For the payload bay, the required volume was selected based on previous experience (28 liters) [18], whereas for the fuel tank the volume is calculated based on the estimated fuel weight, using a typical value for the fuel density (0.68 kg/m^3) [2].

A brief presentation of the three configurations is now made, emphasizing on their distinctive features. The key advantages and disadvantages of each configuration are given, along with simplified drawings and comparative tables to guide the reader through the procedure.

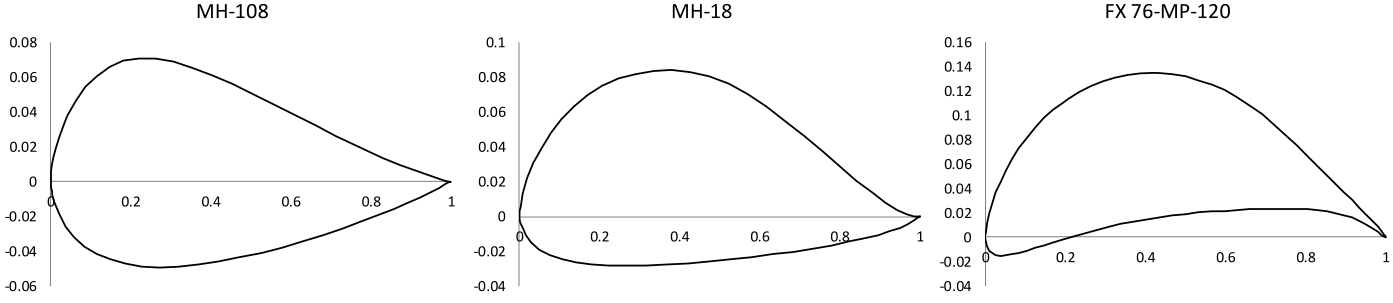

Fig. 8. The selected airfoil profiles.

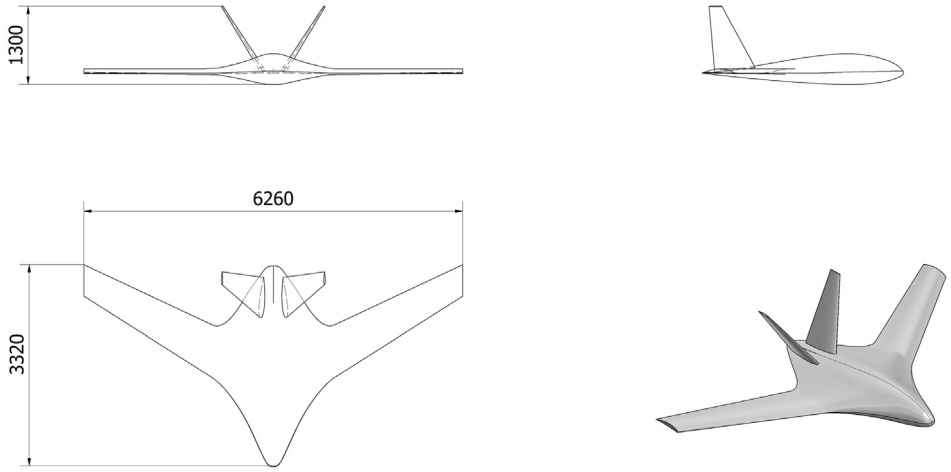

Fig. 9. Configuration #1.

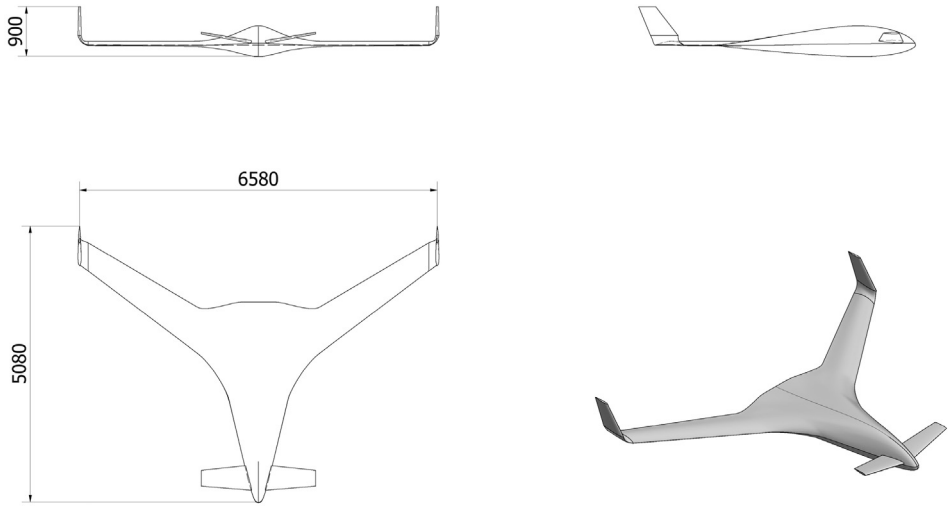

Fig. 10. Configuration #2.

Configuration #1

- The first configuration uses a V tail to provide stability and control for the pitching and yawing axes (Fig. 9). Hence, a set of ruddervators and a set of elevons are used to navigate the UAV.
- Having the more conventional tail arrangement amongst the three, this configuration is expected to be the easier when it comes to handling and mixing each of the surfaces movement to maneuver in-flight.
- Since the tail is responsible for majority of the longitudinal control a smaller sweep angle can be selected (30 deg at the quarter-chord, as opposed to the 35 deg used at the other two configurations), thus improving the aerodynamic performance of the wing.
- The tail is dedicated to the stability and control of the UAV may be a simple and reliable way of solving the control issue, at the same time though it greatly increases the wetted area of the configuration and decreases the overall aerodynamic efficiency of the aerial vehicle.
- The center body is enlarged to provide adequate room for the tail to be installed, leading to an increase in wetted area.

Configuration #2

- The second configuration uses canards for longitudinal control, whereas a set of winglets mounted at the tips of the main wing is used to place the rudders (Fig. 10). Elevon control surfaces are used at the main wing.
- This configuration is expected to have optimum control characteristics. Pitching and yawing control surfaces work independently from each other. Moreover, it is easier for the layout designer to change the distances between the various control surfaces e.g. by changing the location where the canards are mounted on the center body, without causing any large changes on the center body or the wing configuration.
- When compared to the other configurations, this layout has two control surfaces more (six instead of four). This means that two extra servo-actuators are required, which in turn will slightly increase the UAV empty weight, as well as its system complexity.
- The center body is larger in length to provide the necessary lever arm for the canards, thus increasing the total wetted area. Moreover, part of the wing/center body operates inside the wake of the canards that is expected to affect the aerodynamic performance in a negative way.

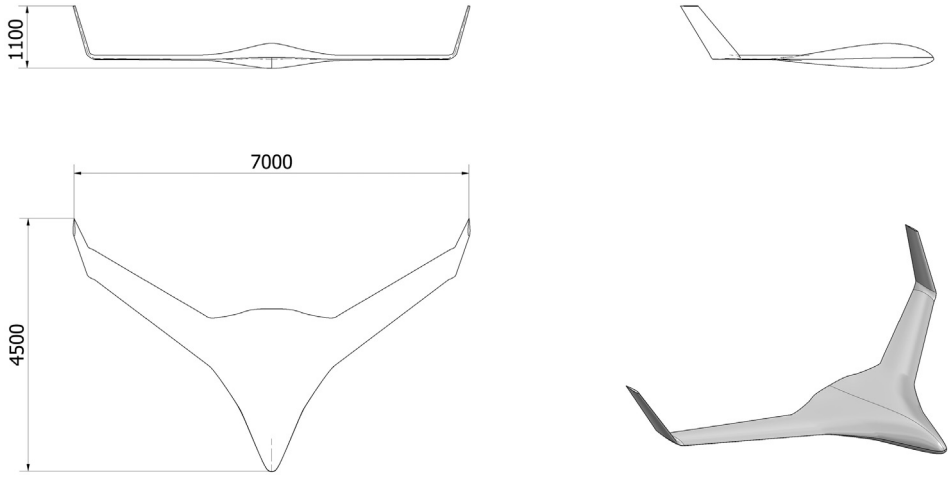

Fig. 11. Configuration #3.

Configuration #3

- In the third configuration, the winglets are used both for pitching and yawing, whereas the elevons are used for pitching and rolling (Fig. 11).
- The center body does not host any control surfaces, therefore its sizing constraints are only related to internal volume requirements.
- This is the only layout amongst the three that can support both a pusher and a tractor engine configuration.
- The large lever resulting from the placement of all control surfaces on the winglets leads to a reduction in the size of the control surfaces. Reduced control surfaces size yields a smaller wetted area.

Towards the end of the conceptual design, and having defined the different BWB configurations, a more refined weight estimation is made [32]. More specifically, the weight of each of the components is estimated from the layout drawings, using the dedicated weight prediction methods. The "General Aviation" methods were employed, as they yield the most accurate estimations for the case of a fixed-wing UAV. The dedicated equations (4) and (5) were also used at this point, to estimate the weight of the wing and center body respectively. By summing up the weight of each of the components, a new estimate for the empty weight ($W_{e,as\ drawn}$) is derived, which in turn is substituted in eq. (8), yielding a new value for the total weight of the aerial vehicle ($W_{0,as\ drawn}$).

Furthermore, a performance assessment is carried out to calculate the performance parameters, compare them with the initial requirements, and ensure that the configurations fulfill the initial requirements and are up to the task. What is more, those performance parameters were also used to compare the three configurations and come up with the most efficient one (Table 5). Since the performance assessment was conducted using some well-established methods [2,32,33] without any special adjustments required for the BWB case, no further analysis will be made in this paper.

The last step is to carry out a last weight estimation based on the methodology described in [32]. An iterative procedure is essentially defined, where the $W_{0,as\ drawn}$ is set as the initial value for the total weight. At first, a new estimation for the fuel weight is calculated based on the more refined aerodynamic coefficient values from the CFD computations. This estimation is in turn added to the other weight components, that is (eq. (11)):

$$W_0 = W_{e,as\ drawn} + W_{f,refined} + W_p \tag{11}$$

Table 4
Layout specifications and weights comparison between the three configurations.

Configuration	#1	#2	#3
Layout data			
Root chord [m]	3.32	3.70	2.90
Total length [m]	3.33	4.78	3.92
Wingspan [m]	6.26	6.58	7.00
Sweep @ c/4 [deg]	30	35	35
Reference area [m^2]	6.85	7.25	6.80
Wetted area [m^2]	16.97	18.68	16.28
No. of control surfaces	4	6	4
Weights			
$W_{0,as\ drawn}$ [kg]	190.33	191.18	189.15
$W_{e,as\ drawn}$ [kg]	118.77	119.62	117.59
W_0 [kg]	198.81	193.13	177.03
W_e [kg]	123.53	120.72	110.79
W_f [kg]	40.29	37.41	31.25
W/S [kg/m^2]	29.02	26.64	26.05

In case the new value of W_0 deviates from the $W_{0,as\ drawn}$ the empty weight component is recalculated using eq. (12) and the procedure is repeated until convergence is reached for the total weight of the aerial vehicle.

$$W_e = W_{e,as\ drawn}\left[\frac{W_0}{W_{0,as\ drawn}}\right]^{(0.9)} \tag{12}$$

This step concludes the rubber engine sizing of the aerial vehicle. It should be noted that the W_0 does not correspond to the as-drawn configuration, it rather represents the potential of the aerial vehicle in case a custom engine was developed.

Table 4 sums up the layout specifications and weight estimations for the three configurations, whereas in Table 5 a detailed performance comparison is made. Starting with the layout characteristics, it is evident that the length and wingspan are of the same order of magnitude, since all three configurations are based on the same MALE UAV mission requirements. The requirement for a large lever arm causes Configuration #2 to be larger in length though, whereas canting the winglets outwards causes Configuration #3 to have a larger wingspan.

Considering the as-drawn values, there is little difference between the empty and, consequently, the total weights since the three configurations have relatively few differences in dimensions. Using the refined rubber engine weight estimation method though, Configuration #3 gets as much as 10% lighter in weight, giving it a considerable advantage. This advantage mainly results from its considerably higher aerodynamic efficiency, as discussed in the following lines, which results in a lower fuel consumption, yields a

Table 5
Aerodynamic and performance specifications comparison between the three configurations.

Configuration	#1	#2	#3
Aerodynamics			
$C_{D,0}$	0.01497	0.01417	0.01336
$C_{L,max}$	1.209	1.2759	1.1914
$(C_L/C_D)_{max}$	17.5	19.3	21.7
Performance			
Maximum speed [km/h]	217.5	220.6	231.8
Stall speed [km/h]	83.6	80.2	79.5
Service ceiling [m]	7500	8100	8700
Rate of climb [ft/m]	730	760	890
Takeoff runway [m]	136	118	106
Min. turn radius [m]	73.23	63.65	55.09
Max. turn rate [deg/s]	21.81	23.90	26.66

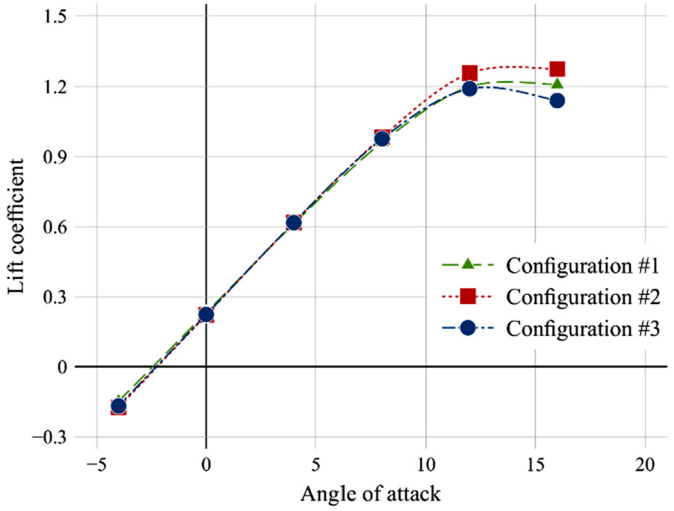

Fig. 12. Lift curve comparison between the three BWB UAV configurations using CFD.

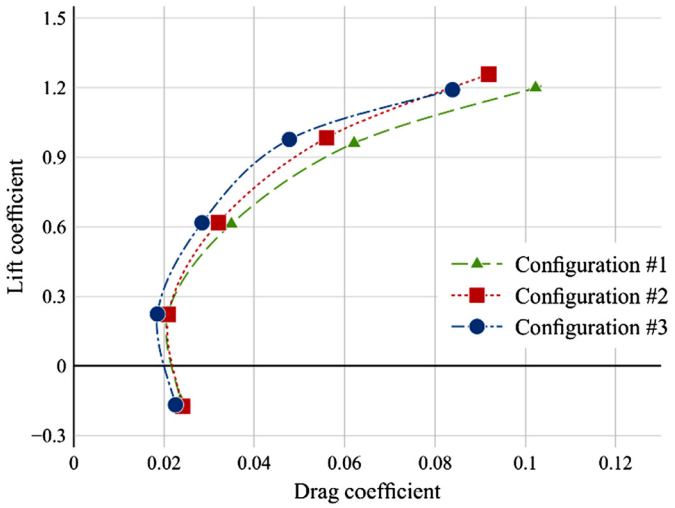

Fig. 13. Drag polar comparison between the three BWB UAV configurations using CFD.

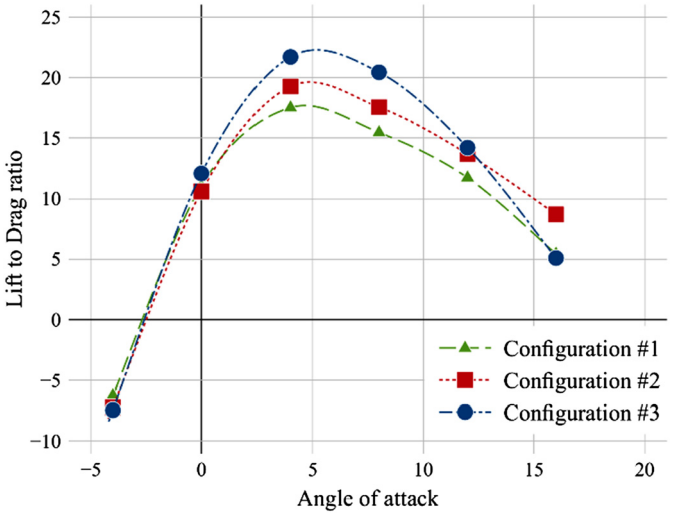

Fig. 14. Lift-to-Drag chart comparison between the three BWB UAV configurations using CFD.

reduction of the total weight of the aerial vehicle and in turn indicates that this configuration layout has better potential as a MALE UAV platform.

In terms of aerodynamics, the data in Table 5 indicate that Configuration #3 has an advantage in cruise-loiter performance due to higher aerodynamic efficiency and lower zero-Lift Drag coefficient ($C_{D,0}$). More specifically, CFD data show that it has the lowest $C_{D,0}$ and highest $(L/D)_{max}$ amongst the three configurations, whereas Configuration #1 has the largest maximum lift coefficient ($C_{L,max}$). As expected, Configuration #1 appears to be the worst in terms of aerodynamic efficiency, due to its large tail surfaces. The above observations can also be made in Figs. 12 to 14, where the aerodynamics comparison is summed up. Moreover, in Fig. 15 the pressure contours over the three configurations are presented, as calculated from CFD.

Performance specifications reflect the above observations and eventually prove the superiority of Configuration #3 in this comparative study. Combining lower wing loading with better aerodynamics, it is clearly the best choice amongst the three BWB configurations in every aspect, from maximum speed to maneuverability. Configuration #2 ranks second, whereas Configuration #1 is the worst amongst the three. Regarding the stall speed, it is evident that none of the configurations meets the initial requirement due to the relatively low $C_{L,max}$. However, the aerodynamics and wing loading of the BWB platforms make up for this deficit since the rest of the mission requirements are met by all three configurations (apart from the maximum velocity of Configuration #1 that falls short of just 3 km/h) indicating that the overall design procedure was properly conducted.

Engine selection

Another important parameter defined during this early design phase is the engine type that best fits the mission of the UAV. Two different types were examined, i.e. a jet engine and a piston engine, and two off-the-self UAV engine models were selected that best fit the thrust/power requirements established in the previous Section. A Zanzoterra 305h (© Zanzoterra Engines) represented the piston engine type, which is an internal combustion engine combined with a propeller, and a PBS TJ40-G1 turbojet (© PBS Velká Bíteš) represented the jet engine type. It should be noted that the available options for this class of aerial vehicles are relatively limited, especially when it comes to the jet engine. Moreover, to acquire some of the features listed in Table 6 a direct contact with the manufacturers was made, due to lack of information on the Internet.

The comparison was carried out using the fixed engine sizing procedure described in [32]. That is, the empty weight equals the value of $W_{e,as\ drawn}$, whereas the W_0 was calculated by multiplying the power/thrust loading with the corresponding engine

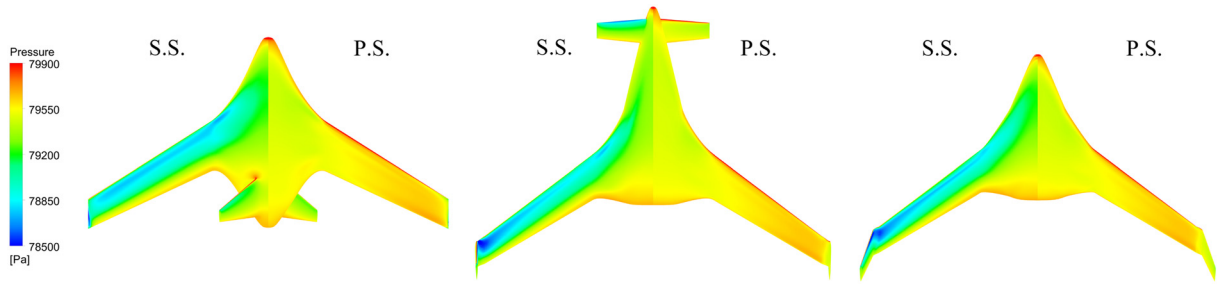

Fig. 15. Pressure development on the surface of the three BWB configurations, as a result of the CFD computations. S.S. and P.S. stand for Suction Side and Pressure Side respectively.

Table 6
Engine comparison.

Engine specifications	Zanzoterra 305h	PBS TJ40-G1
Type of engine	Two-cylinder, two-stroke ICE	Turbojet
Maximum power/thrust	25 hp	395 N
SFC at maximum power/thrust	0.463 kg/hp/h	0.147 kg/N/h
Engine weight with acc.	10.8 kg	3.45 kg
Max. revolutions	7000 rpm	98000 rpm
Temperature	−45 °C to 65 °C	−20 °C to 50 °C
Max. operating altitude	N/A	6000 m

power/thrust (Table 6). The empty and payload weight components are then subtracted from W_0 and the remaining weight is by definition the fuel weight component. More specifically, the resulting fixed engine W_0 values for the turbojet case are larger than those of the ICE for each configuration due to the higher available thrust, thus leading to higher fuel weight values (Table 7). However, the jet engine has a considerably higher Specific Fuel Consumption (SFC), leading ultimately to much lower endurance values. Along with the Takeoff distance (which is lower for the piston engine since the thrust provided at low speeds is higher), those are the two parameters where the ICE performs in a better way. The jet excels at every other parameter yielding a 30–40% enhanced performance.

Summing up, the best type of engine cannot be defined in absolute terms. The jet engine offers significantly better performance in terms of speed and maneuverability, at the cost of fuel consumption and flight time, something that can be of use to a wide variety of missions. It should also be noted at this point though that, according to the information provided by the manufacturers, the ICE is approximately three times cheaper to purchase. Therefore, for the current case, where the primary objective is to design a MALE UAV for surveillance purposes, the ICE was eventually selected.

3.2. Optimization and trade studies

Initial CG calculation

Since, apart from performance and aerodynamics, internal layout and stability were also examined, an initial Center of Gravity (CG) calculation was conducted. It was based on semi-empirical methods described in [2] for the structure, whereas the engine, payload and fuel tank were treated separately. Normalizing the CG location on the longitudinal axis a value of $x_{CG}/c_{root} = 64\%$ was calculated, serving as reference point for the stability considerations presented for the trade studies in this section. A notable conclusion was that the BWB designer can easily tune the CG location after the aerodynamics and performance have been defined, because plenty of space for the various parts to be placed exists.

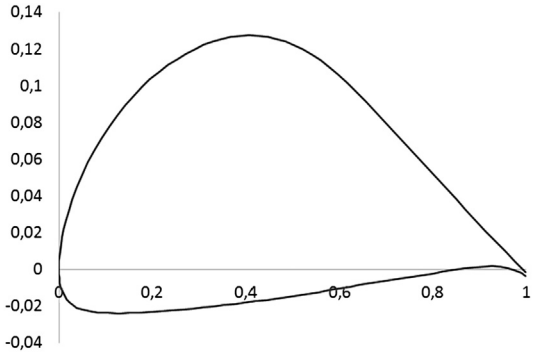

Fig. 16. The AH 94-145 airfoil.

Airfoil trade study

As a start, it was decided to examine the replacement of the reflexed camber airfoil profiles with conventional ones and evaluate the effect such a decision has on the aerodynamic performance and stability of the aerial vehicle. Apart from the airfoil profiles and their respective incidence angle, the rest of the geometrical characteristics were kept constant. Based on aerodynamic efficiency and internal volume requirements, the AH 94-145 airfoil profile was selected (Fig. 16).

The results of the corresponding CFD aerodynamics study are presented in Fig. 17. A large increase in $C_{L,0}$ is observed, as a result of a more negative zero-lift angle of attack, as well as in $C_{L,max}$. This indicates that a lower angle of attack is required for the same lift coefficient to be achieved, which, in the case of the current design is approximately −3 degrees. This is also evident in Fig. 18, where the drag polar has shifted upwards. At same time, though, it has also shifted to the right, due to an increase of $C_{D,0}$. That is, the addition of the conventional airfoils may improve the low-speed performance, thus decreasing the stall speed by 17%, but yields reduced cruise and loiter performance. The most important drawback of this decision though, has to do with longitudinal stability. *A* pitching moment coefficient at zero angle of attack ($c_{m,0}$) of −0.83 and a pitching moment slope ($c_{m,\alpha}$) of −2.9 were calculated based on the estimated center of gravity (Fig. 19). Hence, even though the configuration is stable, the slope is very close to the limits suggested by the literature [41,42], whereas the pitching moment coefficient is too negative, indicating that the UAV should fly trimmed throughout its entire mission. In other words, the nose-down pitching moment produced by the positive cambered airfoils, combined with the absence of a conventional tail leads to excessive trimming requirements. Although a more detailed calculation cannot be made at this point of the design, the corresponding configuration, i.e. the Dash-Two, was dropped as an option for the rest of this study.

Table 7
Fixed engine comparison between the three BWB configurations for both engine types.

Configuration	#1		#2		#3	
Engine type	Jet engine	IC engine	Jet engine	IC engine	Jet engine	IC engine
Fixed engine weights						
W_0 [kg]	189.01	172.56	189.01	172.56	189.01	172.56
$W_{e,as\ drawn}$ [kg]	118.77	118.77	119.62	119.62	117.59	117.59
W_f [kg]	35.24	18.79	34.39	17.94	36.43	19.97
Performance						
Endurance [h]	0.81	4.34	0.84	4.35	1.11	5.76
Maximum speed [km/h]	283.18	218.56	283.17	221.43	301.33	231.95
Stall speed [km/h]	81.69	77.94	79.40	75.87	82.18	78.52
Rate of climb [ft/s]	19.96	14.50	20.02	14.57	21.37	15.17
Takeoff runway [m]	227	98.6	215	91.8	228.7	100.3
Min. turn radius [m]	37.39	52.48	35.21	49.20	37.43	52.08
Max. turn rate [deg/s]	34.95	27.06	36.19	28.18	35.28	27.62

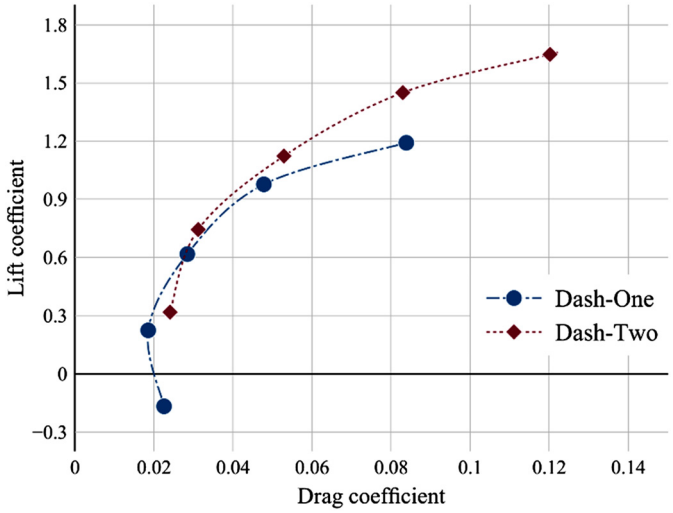

Fig. 17. Drag polar comparison between the configuration with conventional airfoils and the Dash-One using CFD.

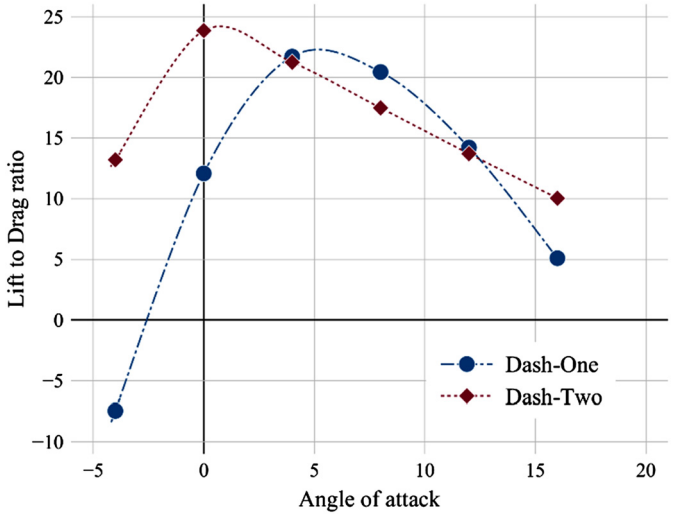

Fig. 18. Lift-to-Drag ratio comparison between the configuration with conventional airfoils and the Dash-One using CFD.

Twist angle optimization

At this part of the study, the geometric twist of the platform was optimized around the loiter lift coefficients to maximize the aerodynamic efficiency of the configuration and to keep the trimming drag at a minimum. More specifically, based on the Dash-One

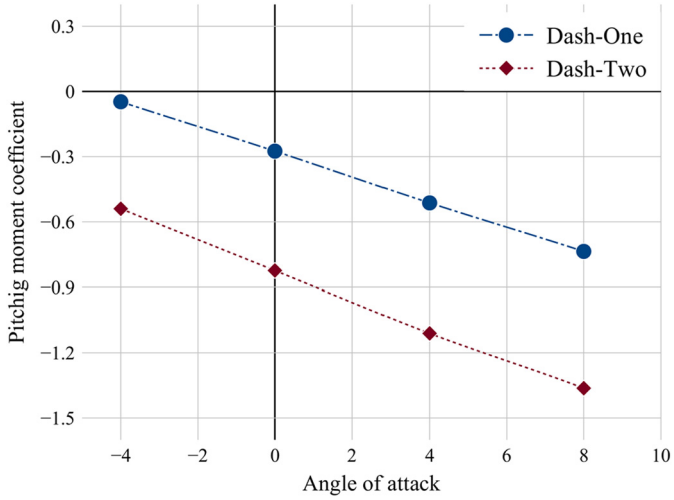

Fig. 19. Pitching moment coefficient comparison between the configuration with conventional airfoils and the Dash-One using CFD.

specifications, a mid-loiter lift coefficient of 0.43 ± 0.05 from start to end was calculated. Then, using 2D low-fidelity tools [43] the lift coefficient of each of the frames was calculated as a function of their respective incidence angle, whereas a correction was also made to take the sweep angle into account [44]. Hence, the local lift versus semi-span chart was drawn (Fig. 20) and an elliptical distribution for the required lift coefficient was achieved over the entire configuration, in a similar methodology as the one presented in [6,34]. Note that y/b is the normalized span, and $C_L \cdot c/c_{ref}$ is the local lift, where c and c_{ref} are the local chord and mean aerodynamic chord lengths respectively.

The last step at this conceptual design phase was to make a few minor changes at the layout by shifting the center body aftwards and rearranging the internal parts to bring the CG at the desired location. The engine was placed at the rear, at a pusher configuration, whereas the front part of the center body was defined as the payload bay. Regarding the fuel, placing it at the wings between the frontal and the rear spar was initially considered as an option to distribute the loads and reduce structural weight. However, the presizing tools cannot predict this weight reduction, whereas placing the fuel away from the symmetry plane increases the moment of inertia and, in turn, the control surfaces requirements. A definite answer would require more advanced tools, therefore the fuel tank in this conceptual phase was placed at the center body and an iterative procedure was carried out so that the fuel tank CG location coincides with CG location of the entire configuration. A x_{CG}/c_{root} of 60% was eventually achieved, ensuring that the final configuration is inherently stable. Following the aforementioned changes,

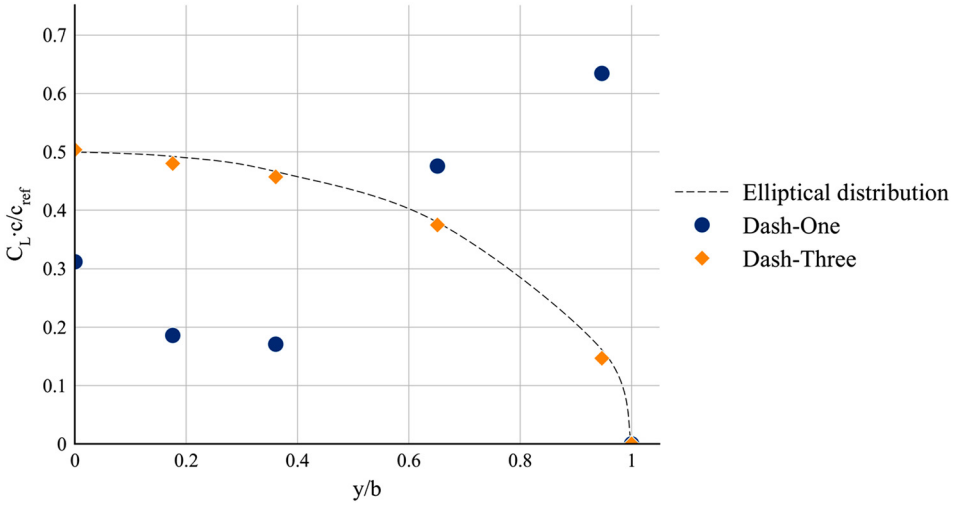

Fig. 20. Dash-One versus optimized lift distribution. The target lift distribution is also shown (dashed line).

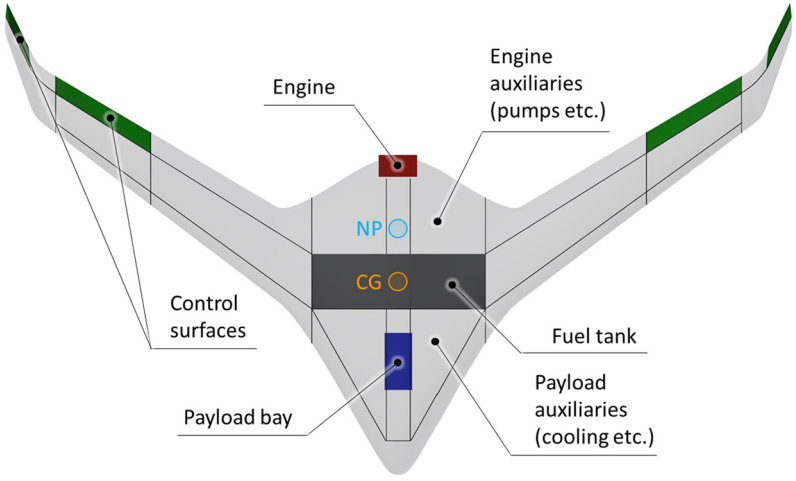

Fig. 21. Dash-Three internal layout. The location of the fuel tank, control surfaces, engine and payload, as well as their auxiliaries, are shown, whereas the black lines are an indicative concept of the structural layout.

the Dash-Three configuration was drawn and the corresponding internal layout is presented in Fig. 21, along with the CG and Neutral Point (NP) longitudinal locations.

Fig. 22 presents the drag polar as calculated from the CFD computations, always in comparison with the Dash-One configuration. As is evident, the Drag polar has shifted upwards so that the minimum drag coefficient is achieved at the desired lift coefficients. Figs. 23 and 24 show the comparison in Lift-to-Drag ratio and the pitching moment coefficient as a function of angle of attack. More specifically, a 4.6% increase in maximum Lift-to-Drag ratio was achieved and it can be observed that the Dash-Three curve has shifted to the left, so that the bigger ratios correspond to the operational angles of attack. Regarding the pitching moment coefficients, the $c_{m,0}$ and $c_{m,\alpha}$ were calculated equal to -0.03 and -2.5/rad based on the CG-NP locations, values that were considered acceptable for conceptual design phase based on literature guidelines. Summing up, the Dash-Three is an overall better configuration and successfully replaced the Dash-One.

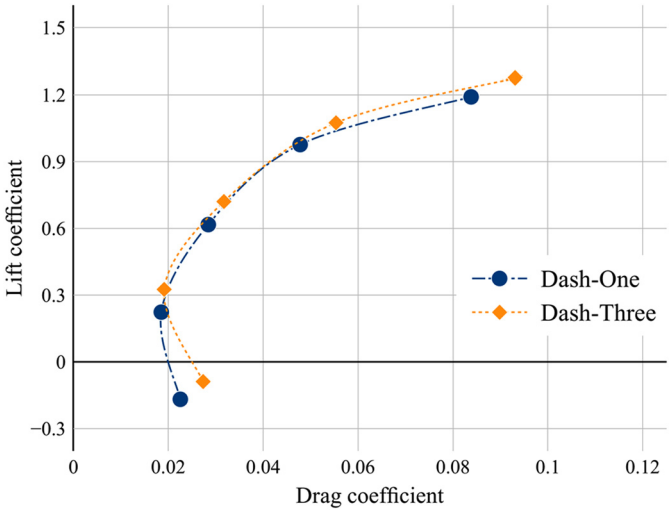

Fig. 22. Dash-Three Drag Polar as calculated from CFD. A comparison with the Dash-One is also made.

Mission type trade study

As also mentioned in the previous section, there is a lot of space available for payload and fuel inside the BWB. Hence, in this trade study three different scenarios regarding the fuel available inside the fuel tank were investigated. The first scenario corresponded to a fuel amount for 5 hours of loiter endurance, the second to a fuel amount for 10 hours of loiter endurance and the third scenario was to completely fill the fuel tank.

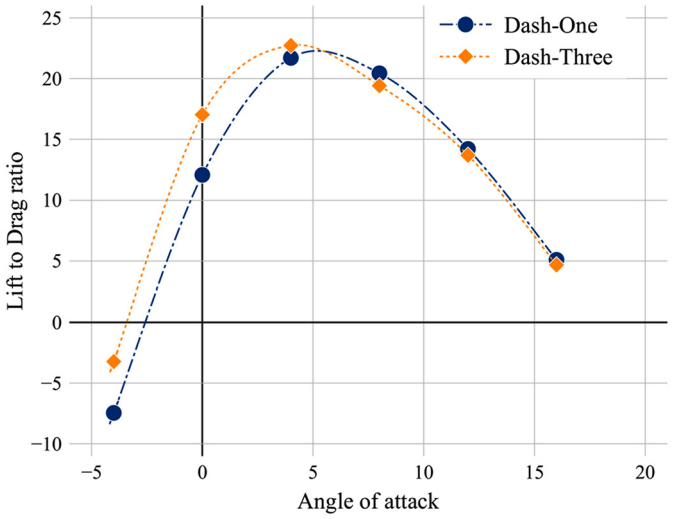

Fig. 23. Lift-to-Drag as a function of angle of attack, calculated from CFD. Comparison between the Dash-Three and Dash-One configurations.

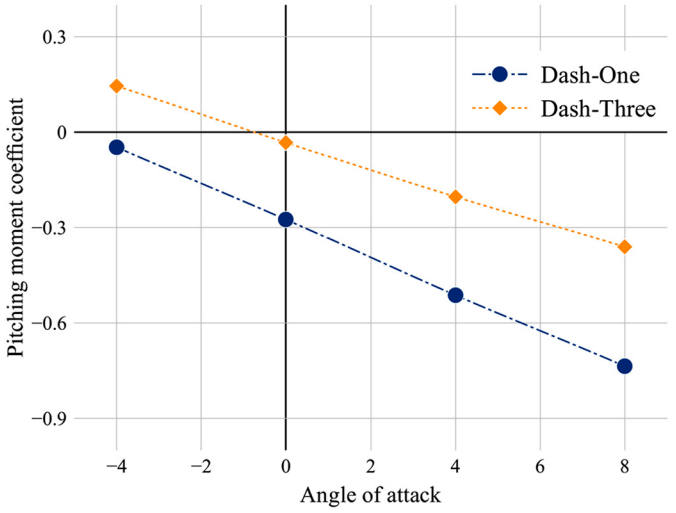

Fig. 24. Pitching moment coefficient as a function of angle of attack, calculated from CFD. Comparison between the Dash-Three and Dash-One configurations.

The results are shown in Table 8, where the effect of the fuel weight on the performance of the platform is essentially examined. Since the CG of the fuel tank coincides with the CG location of the entire configuration, no stability-related information is given. It should be noted at this point that, even though the presizing calculations yield a relatively large value for the net weight, the aerodynamic efficiency of the platform is considerably high. Hence, the BWB UAV configuration is better fitted for long endurance (i.e. greater than 10 hours) missions, where the platform is better exploited.

Final configuration and comparison

The final configuration of this BWB MALE UAV conceptual design study is presented in Fig. 25. The corresponding performance specifications are presented in Table 9, where a comparison with a conventional UAV configuration is also made. More specifically, the HCUAV was employed and its loiter endurance, calculated at 11 hours with the same in-house presizing tools, served as a reference point [18]. That is, the fuel tank of the BWB configuration was also "filled up" to 11 hours of flight endurance and the rest of the performance specifications were calculated for the corresponding W_0 value. Once again, the aerodynamics comparison was based on

Table 8
Mission type trade study.

Endurance	5 h	10 h	Full tank
Final weights			
W_e [kg]	117.6	117.6	117.6
W_f [kg]	16.5	29.2	59.8
W_0 [kg]	169.1	181.8	212.4
W/S [kg/m^2]	24.7	26.5	31
Performance			
Endurance [h]	5.0	10.0	21.4
$(C_L/C_D)_{max}$	20.3	20.3	20.3
Maximum speed [km/h]	228.2	227.7	226.3
Stall speed [km/h]	71.7	74.3	80.7
Rate of climb [ft/s]	915	837	685
Takeoff runway [m]	90	105	148
Min. turn radius [m]	50.12	59.17	85.83
Max. turn rate [deg/s]	28.12	25.32	19.86

Table 9
Fixed engine comparison between the three BWB configurations for both engine types.

Specifications	BWB	HCUAV RX-1
W_0 [kg]	190.5	185
W_f [kg]	39.3	55
W_p [kg]	35	35
W/S [kg/m^2]	38.9	41.5
Endurance [h]	11.0	11.0
Maximum speed [km/h]	210	190
Stall speed [km/h]	79	70
Rate of climb [ft/m]	700	550
Takeoff runway [m]	136	130

CFD. The extra drag, e.g. from the gimbal and landing gear, was taken into account using the spreadsheet methods described in [33] and resulted in a slight decrease in the BWB performance. A screenshot from the CFD analyses at the BWB configuration is indicatively shown in Fig. 26, where the streamlines around the platform are shown for 8°, whereas an overlaid top view of the BWB and the conventional UAV configurations is shown in Fig. 27.

Moreover, Figs. 28 and 29 present the Drag Polar and aerodynamic efficiency charts of the final BWB UAV configuration in comparison to the HCUAV RX-1. The superiority of the BWB is evident, since the $C_{D,0}$ is reduced by approximately 30% and the Lift-to-Drag ratio is better at almost every angle of attack, with the $(L/D)_{max}$ reaching a difference at the order of magnitude of 15%.

Summing up, the BWB outperforms the conventional configuration in almost every aspect, and especially in fuel consumption, maximum speed and rate of climb, whereas the deficit in stall speed has only a minor impact on the required takeoff runway. Apart from aerodynamics and performance though, the BWB configuration has a clear advantage when it comes to the internal volume available, a feature that greatly adds to the versatility of a UAV platform. Moreover, a BWB UAV designer could also investigate the installation of solar panels, due to the increased available area, or the use of hydrogen fuel cells, which are generally lighter in weight but require more space than a conventional fuel tank [45].

The resulting configuration is by no means an all-round optimized design. Moving on to a more advanced design phase, an external layout optimization using an Multidisciplinary Optimization (MDO) approach could aid in further increasing the aerodynamic efficiency and the calculation of the stability derivatives could aid in fine-tuning the stability and control characteristics of the aerial vehicle. A trim diagram is also necessary to optimize the in-flight performance, whereas an optimization from a structural point of view, judging from previous experience [46], could result in a reduction in total weight at the order of magnitude of 10%, further increasing the performance specifications of the BWB MALE UAV.

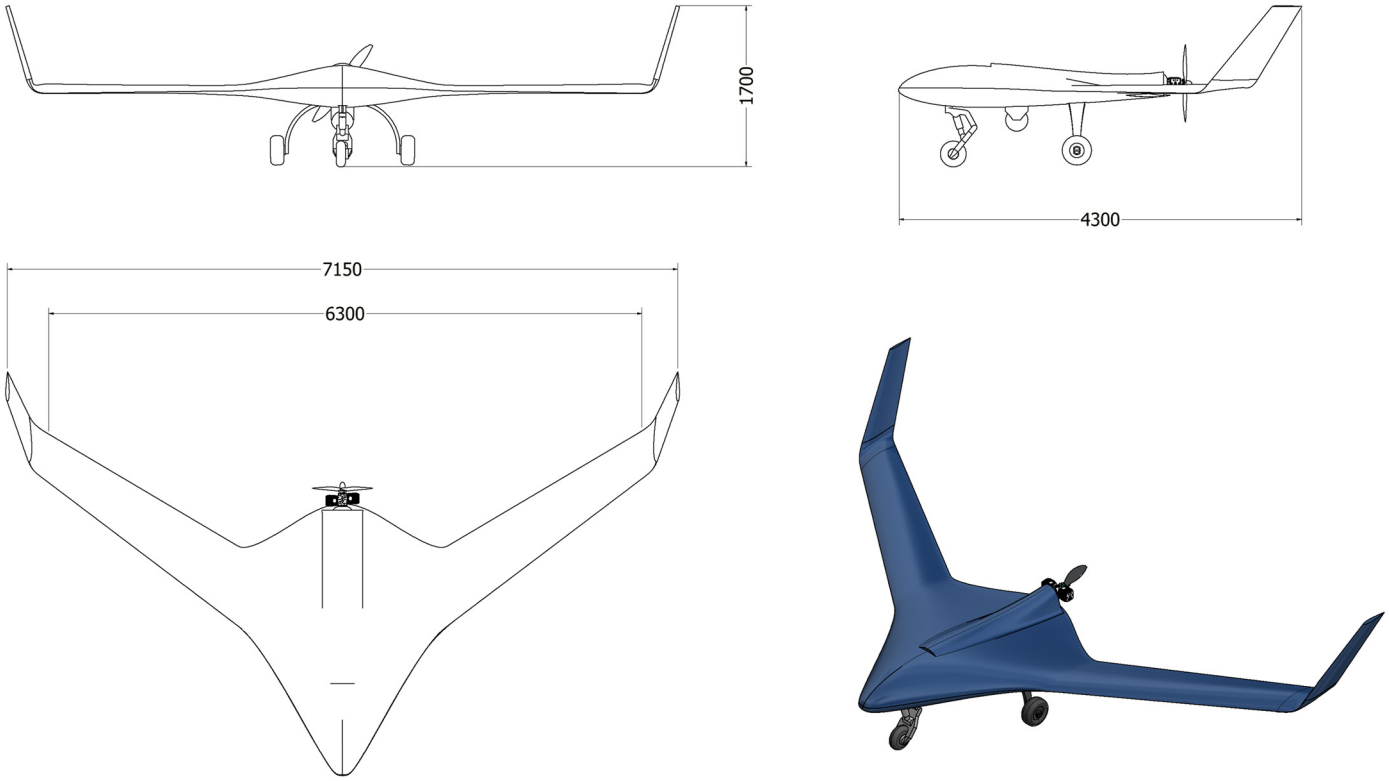

Fig. 25. CAD representation of the final configuration.

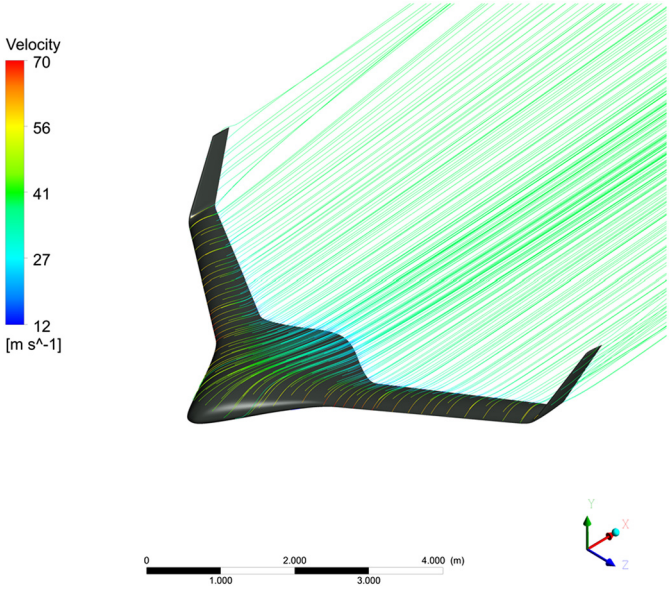

Fig. 26. Streamlines around the BWB Dash-Three configuration at 8°.

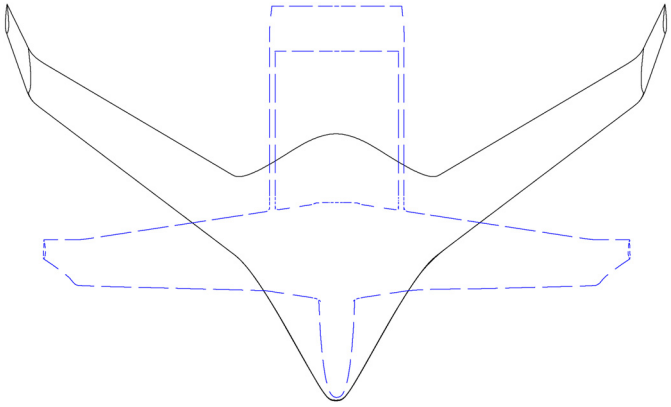

Fig. 27. Overlaid top view of the BWB Dash-Three (black solid line) and HCUAV RX-1 (blue dashed line) configurations.

4. Conclusions

In the present work, the conceptual design and sizing of a BWB fixed-wing MALE UAV was performed. The design procedure was based on an in-house presizing tool, whereas CFD computations were also conducted to accurately calculate the aerodynamic and stability coefficients. Due to the innovative aspects of the BWB platform, adjustments were made to existing sizing methods, emphasizing on the layout considerations, weight prediction methods and aerodynamic analysis methods.

At first, the initial presizing calculations were carried out, yielding the initial weight and performance parameter estimations. A layout selection procedure was then conducted to define the optimal configuration for the mission. More specifically, three different BWB-based layouts were drawn, each having a different concept regarding the stability and control. By using the presizing tools, CAD models and CFD analyses, the configurations were examined and compared in terms of weights, aerodynamics and performance to select the optimal one. Using a fixed-engine approach, the engine type that best fits the requirements of the MALE UAV was in turn selected, with the ICE being chosen over the jet one. Hence, a propeller driven, pusher BWB layout with control surfaces at the winglets for pitch and yaw control was eventually selected, marked as the Dash-One. Furthermore, a couple of CFD-aided optimization and trade studies were conducted to fine-tune the performance of the UAV at a conceptual level. A preliminary calculation showed that the center of gravity of a BWB UAV configuration can be easily adjusted due to the large internal volume available. The use of conventional instead of reflexed camber air-

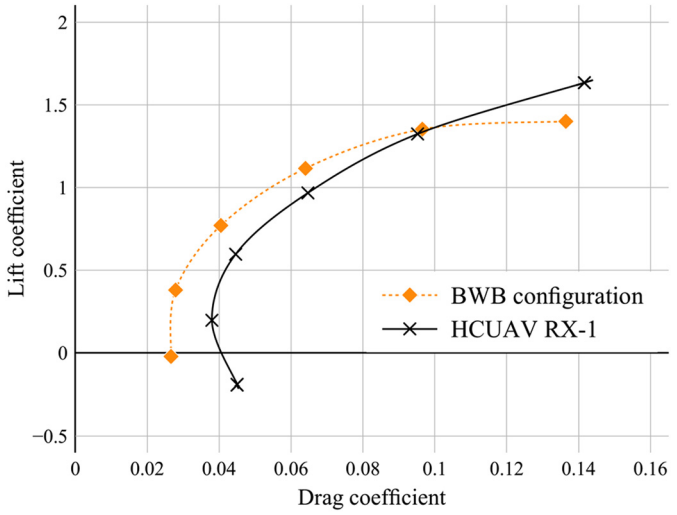

Fig. 28. Drag polar comparison between the BWB Dash-Three and the HCUAV RX-1 MALE UAVs, using CFD.

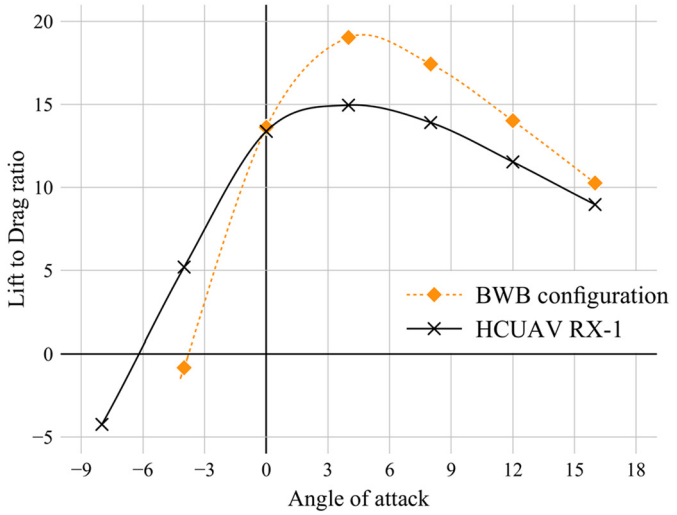

Fig. 29. Lift-to-Drag ratio comparison between the BWB Dash-Three and the HCUAV RX-1 MALE UAVs, using CFD.

foils was examined, however this scenario was dropped due to the large pitching moment penalty and the relatively small benefit in aerodynamics. The lift distribution and twist angle was adjusted to optimize the performance of the aerial vehicle in loiter conditions thus maximizing the L/D and keeping the trim requirements at a minimum. In the end, a more refined CG calculation was conducted, whereas minor changes in the layout ensured an inherently stable design. Summing up:

- The conceptual design of a BWB requires some adjustments to be made both in the sizing tools and the layout philosophy. Especially considering the former, not enough examples of operating BWBs are available to calibrate the semi-empirical models.
- Although not optimal in terms of aerodynamic efficiency, a large sweep angle at the order of magnitude of 35 degrees is required to ensure a positive static margin and adequate controllability.
- Avoiding extra surfaces dedicated to control, such as fins and canards, is the optimal solution in terms of aerodynamics. The optimal configuration of this study has a set of elevons at the wings for combined pitch and roll control, whereas yaw control is achieved using control surfaces at the winglets. Slightly canted outwards, the latter also aid in pitch control. Namely, getting rid of the extra surfaces yields a decrease in $C_{D,0}$ and an increase in $(L/D)_{max}$ of up to 12.1% and 24% respectively.
- For a UAV of that size, both an ICE and a jet engine can be used. The jet may outperform the ICE in most of the performance criteria, but the ICE yields the flight endurance required for surveillance operations at a far more reduced cost in terms of fuel weight.
- Stability considerations force the use of reflexed camber airfoils in the case of a BWB UAV, at least for the center body airfoil profiles. The corresponding penalty in aerodynamic efficiency is at the order of magnitude of 10%.
- When compared to a conventional UAV configuration the difference in aerodynamic efficiency is at the order of magnitude of 30%. This is reflected to most of the performance parameters and, in combination with the large available internal volume, it can be concluded that the BWB is a much promising platform for UAV applications.

Concluding, the purpose of this study was not to develop an all-round optimized configuration but to answer the key design issues encountered in the conceptual design phase. Based on the results and the potential of the BWB configuration for MALE UAVs, the authors have a number of suggestions for future work to help address some remaining research topics, mainly related to more advanced design phases. Indicatively, even though adjustments were made to the presizing methodology, the empty weight estimation formulas can be further refined. Since the BWB is a relatively innovative configuration with only but a few operating examples, a thorough structural study is suggested to more accurately estimate the empty weight. An optimization in terms of structural layout could help remove the extra structural weight, further enhancing the performance characteristics of the aerial vehicle. Moreover, the fact that the control surfaces layout of the proposed configuration deviates considerably from the conventional ones, suggests that a stability and control oriented study should be conducted to check the state-of-the-art methods related to stability derivatives calculation and flight control algorithms and, if necessary, adjust them to the case of a BWB UAV. Finally, and since the key parameters of the layout have been defined, a Multidisciplinary Optimization study could help towards designing an optimized BWB MALE UAV.

Conflict of interest statement

The authors declare that no conflict of interest exists.

References

[1] R.H. Liebeck, Design of the blended wing body subsonic transport, J. Aircr. 41 (2004) 10–25, https://doi.org/10.2514/1.9084.
[2] J.D. Anderson, Aircraft Performance and Design, WCB/McGraw–Hill, Boston, Mass., 1999.
[3] J. van Dommelen, R. Vos, Conceptual design and analysis of blended-wing-body aircraft, Proc. Inst. Mech. Eng., G J. Aerosp. Eng. 228 (2014) 2452–2474, https://doi.org/10.1177/0954410013518696.
[4] M. Voskuijl, G. La Rocca, F. Dircken, Controllability of blended wing body aircraft, in: Proceedings of the 26th International Congress of the Aeronautical Sciences, ICAS 2008, Anchorage, Alaska, 2008.
[5] S. Siouris, N. Qin, Study of the effects of wing sweep on the aerodynamic performance of a blended wing body aircraft, Proc. Inst. Mech. Eng., G J. Aerosp. Eng. 221 (2007) 47–55, https://doi.org/10.1243/09544100JAERO93.
[6] N. Qin, A. Vavalle, A. Le Moigne, M. Laban, K. Hackett, P. Weinerfelt, Aerodynamic considerations of blended wing body aircraft, Prog. Aerosp. Sci. 40 (2004) 321–343, https://doi.org/10.1016/j.paerosci.2004.08.001.
[7] P. Li, B. Zhang, Y. Chen, C. Yuan, Y. Lin, Aerodynamic design methodology for blended wing body transport, Chin. J. Aeronaut. 25 (2012) 508–516, https://doi.org/10.1016/S1000-9361(11)60414-7.
[8] Z. Lyu, J.R.R.A. Martins, Aerodynamic design optimization studies of a blended-wing-body aircraft, J. Aircr. 51 (2014) 1604–1617, https://doi.org/10.2514/1.C032491.

[9] H. Engels, W. Becker, A. Morris, Implementation of a multi-level optimisation methodology within the e-design of a blended wing body, Aerosp. Sci. Technol. 8 (2004) 145–153, https://doi.org/10.1016/j.ast.2003.10.001.
[10] R. Wittmann, Passenger acceptance of BWB configurations, in: Proceedings of the 24th International Congress of the Aeronautical Sciences, ICAS 2004, Yokohama, Japan, 2004.
[11] N.P. Yovanof, A. Velicki, V. Li, Advanced structural stability analysis of a noncircular, BWB-shaped vehicle, in: Proceedings of the 50th AIAA/ASME/ASCE/AHS/ASC Structures, Structural Dynamics and Materials Conference, Structures, Structural Dynamics, and Materials and Co-located Conferences, 2009.
[12] E.R. Galea, L. Filippidis, Z. Wang, J. Ewer, Fire and evacuation analysis in BWB aircraft configurations: computer simulations and large-scale evacuation experiment, Aeronaut. J. 114 (2010) 271–277, https://doi.org/10.1017/S0001924000003717.
[13] R. Vos, F.J.J.M.M. Geuskens, M.F.M. Hoogreef, A new structural design concept for blended wing body cabins, in: Proceedings of the 53rd AIAA/ASME/ASCE/AHS/ASC Structures, Structural Dynamics and Materials Conference, Structures, Structural Dynamics, and Materials and Co-located Conferences, 2012.
[14] Boeing: Blended Wing Body Goes with the Flow in New Visualization Test, http://www.boeing.com/features/2017/05/blended-wing-body-05-17.page.
[15] R.C. Odle, D. Roman, B.K. Rawdon, Blended wing body cargo airplane, http://www.google.com/patents/US20110121130, 2011.
[16] K. Lehmkuehler, K.C. Wong, D. Verstraete, Design and test of a UAV blended wing body configuration, in: Proceedings of the 28th Congress of the International Council of the Aeronautical Sciences, ICAS 2012, Brisbane, Australia, 2012.
[17] R. Austin, Unmanned Aircraft Systems, UAVS Design, Development and Deployment, Wiley, Chichester, West Sussex, United Kingdom, 2010.
[18] P. Panagiotou, P. Kaparos, C. Salpingidou, K. Yakinthos, Aerodynamic design of a MALE UAV, Aerosp. Sci. Technol. 50 (2016) 127–138, https://doi.org/10.1016/j.ast.2015.12.033.
[19] P. Panagiotou, P. Kaparos, K. Yakinthos, Winglet design and optimization for a MALE UAV using CFD, Aerosp. Sci. Technol. 39 (2014) 190–205, https://doi.org/10.1016/j.ast.2014.09.006.
[20] P. Panagiotou, I. Tsavlidis, K. Yakinthos, Conceptual design of a hybrid solar MALE UAV, Aerosp. Sci. Technol. 53 (2016) 207–219, https://doi.org/10.1016/j.ast.2016.03.023.
[21] S. Chiesa, M. Fioriti, R. Fusaro, MALE UAV and its systems as basis of future definitions, Aircr. Eng. Aerosp. Technol. 88 (2016) 771–782, https://doi.org/10.1108/AEAT-08-2014-0131.
[22] S. Rajagopal, R. Ganguli, Conceptual design of UAV using Kriging based multi-objective genetic algorithm, Aeronaut. J. 112 (2008) 653–662.
[23] R. Ganguli, S. Rajagopal, Multidisciplinary design optimization of an UAV wing using Kriging based multi-objective genetic algorithm, in: Proceedings of the 50th AIAA/ASME/ASCE/AHS/ASC Structures, Structural Dynamics, and Materials Conference, Structures, Structural Dynamics, and Materials and Co-located Conferences, 2009.
[24] R.M. Ajaj, M.I. Friswell, W.G. Dettmer, A.T. Isikveren, G. Allegri, Conceptual modeling of an adaptive torsion wing structure, in: Proceedings of the 52nd AIAA/ASME/ASCE/AHS/ASC Structures, Structural Dynamics and Materials Conference, Structures, Structural Dynamics, and Materials and Co-located Conferences, 2011.
[25] Viking 400-S datasheet, http://www.uadrones.net/military/research/acrobat/100722-b.pdf, 2009.
[26] U.S. Air Force Fact Sheet: MQ-1B PREDATOR, https://web.archive.org/web/20130624094111/http://www.af.mil/information/factsheets/factsheet_print.asp?fsID=122&page=1.
[27] Y. Gibbs, NASA Armstrong Fact Sheet: Altus II, http://www.nasa.gov/centers/armstrong/news/FactSheets/FS-058-DFRC.html.
[28] H.J. Shim, S.O. Park, Low-speed wind-tunnel test results of a BWB-UCAV model, Proc. Eng. 67 (2013) 50–58, https://doi.org/10.1016/j.proeng.2013.12.004.
[29] W. Wisnoe, R.M. Nasir, W. Kuntjoro, A.M.I. Mamat, Wind Tunnel experiments and CFD analysis of Blended Wing Body (BWB) Unmanned Aerial Vehicle (UAV) at Mach 0.1 and Mach 0.3, in: Proceedings of the Thirteenth International Conference on Aerospace Sciences & Aviation Technology, ASAT 2009, 2009, pp. 26–28.
[30] W. Wisnoe, W. Kuntjoro, F. Mohamad, R.E.M. Nasir, N.F. Reduan, Z. Ali, Experimental results analysis for UiTM BWB baseline-I and baseline-II UAV running at 0.1 Mach number, Int. J. Mech. 4 (2010) 23–32.
[31] P. Panagiotou, K. Yakinthos, Parametric aerodynamic study of Blended-Wing-Body platforms at low subsonic speeds for UAV applications, in: 35th AIAA Applied Aerodynamics Conference, American Institute of Aeronautics and Astronautics, 2017.
[32] D.P. Raymer, Aircraft Design: A Conceptual Approach, American Institute of Aeronautics and Astronautics, Reston, VA, 2012.
[33] J. Roskam, Airplane Design, DARcorporation, Lawrence, Kansas, 2004.
[34] P. Heinemann, P. Panagiotou, P. Vratny, S. Kaiser, M. Hornung, K. Yakinthos, Advanced tube and wing aircraft for year 2050 timeframe, in: 55th AIAA Aerospace Sciences Meeting, 2017, p. 1390.
[35] P.R. Spalart, S.R. Allmaras, A one-equation turbulence model for aerodynamic flows, in: 30th Aerospace Sciences Meeting & Exhibit, American Institute of Aeronautics and Astronautics, Reno, NV, 1992, pp. 5–21.
[36] P.R. Spalart, C.L. Rumsey, Effective inflow conditions for turbulence models in aerodynamic calculations, AIAA J. 45 (2007) 2544–2553.
[37] A. Sóbester, A.J. Keane, J. Scanlan, N.W. Bressloff, Conceptual design of UAV airframes using a generic geometry service, AIAA Infotech Aerosp. (2005) 26–29.
[38] J. Koster, G. Soin, Hyperion – three years of novel aircraft design, in: Proceedings of the 55th AIAA/ASME/ASCE/AHS/ASC Structures, Structural Dynamics and Materials Conference, Structures, Structural Dynamics, and Materials and Co-located Conferences, 2014.
[39] P.J. Hoe, N.A.R.N. Mohd, Numerical prediction of blended wing body aerodynamic characteristics at subsonic speed, J. Teknol. 71 (2014).
[40] D. Thompson, J. Feys, M. Filewich, S. Abdel-Magid, D. Dalli, F. Goto, The design and construction of a blended wing body UAV, in: 49th AIAA Aerospace Sciences Meeting including the New Horizons Forum and Aerospace Exposition, American Institute of Aeronautics and Astronautics, 2011, https://doi.org/10.2514/6.2011-841.
[41] M.H. Sadraey, Aircraft Design: A Systems Engineering Approach, Wiley, Chichester, 2013.
[42] R. Nelson, Flight Stability and Automatic Control, McGraw–Hill Science/Engineering/Math, Boston, Mass., 1997.
[43] XFLRv5, http://www.xflr5.com/xflr5.htm.
[44] Lloyd R. Jenkinson, Paul Simpkin, Darren Rhodes, Civil Jet Aircraft Design, 1st edition, ISBN 9780340741528, http://store.elsevier.com/product.jsp?locale=en_AU&isbn=9780340741528.
[45] K. Johnson, M.J. Veenstra, D. Gotthold, K. Simmons, K. Alvine, B. Hobein, D. Houston, N. Newhouse, B. Yeggy, A. Vaipan, T. Steinhausler, A. Rau, Advancements and opportunities for on-board 700 bar compressed hydrogen tanks in the progression towards the commercialization of fuel cell vehicles, SAE Int. J. Alt. Power. 6 (2017), https://doi.org/10.4271/2017-01-1183.
[46] P. Panagiotou, E. Giannakis, G. Savaidis, K. Yakinthos, Aerodynamic and structural design for the development of a MALE UAV, in: Proceedings of the 6th EASN International Conference, Porto, Portugal, 2016.